Supplementary materials:

Synthesis, structure, photo- and electro-luminescence of an iridium(III) complex with novel carbazole functionalized β-diketone ligand

Tianzhi Yu[*, 1ξ], Yan Cao[2ξ], Wenming Su[3], Chengcheng Zhang[1], Yuling Zhao[1], Duowang Fan[1], Mingjun Huang[2], Kan Yue[2], Stephen Z. D. Cheng[*, 2]

[1]Key Laboratory of Opto-Electronic Technology and Intelligent Control (Ministry of Education), Lanzhou Jiaotong University, Lanzhou 730070, P. R. China

[2]College of Polymer Science and Polymer Engineering, The University of Akron, Ohio, 44325, USA

[3]Printable electronics research center, Suzhou Institute of Nano-Tech and Nano-Bionics, Chinese Academy of Sciences, Suzhou 215123, China

[*] Corresponding Authors.
Dr. Tianzhi Yu, E-mail: yutianzhi@hotmail.com. Tel. +86-931-4956935; Fax: +86-931-4938756;
Dr. Stephen Z. D. Cheng, E-mail: scheng@uakron.edu. Phone: (330) 972-6931, Fax: (330) 972-8626
[§]These authors are contributed equally.

The structure determination of Ir(^{1}L)$_2$(^{2}L)

The *a** and *b** axes are marked in Fig. 3b and the angle γ* between these *a** and *b** axes in the reciprocal space is measured to be 90°. Therefore, *1/a* and *1/b* values are assumed to be 0.4926 nm^{-1} and 0.9804 nm^{-1}, and the dimensions of the *a* and *b* values in the real space are thus 2.03 nm and 1.02 nm, respectively. In order to obtain the remaining cell parameters of the Ir(^{1}L)$_2$(^{2}L) crystal, such as *c* axis, α and β angles, the Ir(^{1}L)$_2$(^{2}L) single crystal is rotated around the *a** axis of the single crystal to obtain various SAED patterns with different zones of [0kl]. Fig. S1 includes both experimental SAED patterns and their corresponding computer simulated patterns generated from the Cerius^2 software. Fig. S1a is a SAED pattern that is rotated from Fig. 3b to make *a** axis pointing horizontally as a tilting axis. A 33° anticlockwise tilting around the *a** axis results in a SAED pattern with the [011] zone as shown in Fig. S1b. In Fig. S1c, an identical electron diffraction pattern with the [01$\bar{1}$] zone clearly shows the diffraction spot of 011 when the single crystal is tilted 33° clockwise around the same *a** axis. Because both the [011] zone and the [01$\bar{1}$] zone are symmetric around the *b** axis, its unit cell in the real space must also be symmetric, the Ir(^{1}L)$_2$(^{2}L) crystal structure is thus proposed to have an orthorhombic unit cell. This identification is further confirmed by continuously tilting the single crystal to higher angles around the *a** axis. The 012 diffraction spot appears in the ED pattern with the [02$\bar{1}$] zone as shown in Fig. S1d when the crystal was rotated 53° clockwise around the *a** axis. In principle, the 0$\bar{1}$2, 1$\bar{1}$2 diffraction spot is observed in the ED pattern with the [021] zone when the crystal was rotated anticlockwise 53º around the *a** axis (Fig. S1e). But 0$\bar{1}$2 diffraction spot does not show up both in experiment and simulation pattern due to the specific molecular spatial arrangement of Ir(^{1}L)$_2$(^{2}L) in the unit cell. The symmetric nature of the ED patterns with the

[021] and the [02$\bar{1}$] zones around the *b** axis again confirms that the unit cell in the real space is also symmetric around the *b** axis. Finally, the 013 diffraction spot appears in the electron diffraction pattern with the [03$\bar{1}$] zone when the Ir(^{1}L)$_2$(^{2}L) single crystal was rotated 60° clockwise around the *a** axis (Fig. S1f). The summary of all the above mentioned diffraction spots and the corresponding zone axis are illustrated in Fig. S2. Combining the d-spacing calculations and the crystal tilting angles, the unit cell parameter of Ir(^{1}L)$_2$(^{2}L) single crystal can be determined to be a = 2.03 nm, b = 0.99 nm, c = 1.49 nm, α = β = γ = 90°.

The simulated ED patterns with the [010] zone, the [011] zone, the [01$\bar{1}$] zone, the [02$\bar{1}$] zone, the [021] zone, and the [03$\bar{1}$] zone are also shown in Figs. S1a – S1f, respectively. When the Ir(^{1}L)$_2$(^{2}L) crystal was tilted along the *a** axis within the bc plane, the Miller indices of diffraction spots in the *a** axis, such as 100, 200, 300, 400, 500 etc., do not change with the crystal rotation. However, the Miller indices in the *b** axis, such as 010 has changed to 0$\bar{1}$1, 011, 012, 0$\bar{1}$2, 013 corresponding to 33° anticlockwise, 33° clockwise, 53° clockwise, 53° anticlockwise, 60° clockwise crystal tilting, respectively. In addition, the *1/d* values in the reciprocal lattice become bigger when the crystal was increasingly tilted to higher angles. The reason for the increased *1/d* value in the reciprocal lattice is that when the crystal is tilted to a higher angle, in the real space, the smaller d-spacing corresponds to a higher Miller index. Overall, the simulated patterns are in good accordance with the experimental results, confirming that the predicted structure parameters and space group of the Ir(^{1}L)$_2$(^{2}L) single crystal are reasonable to represent the real crystal structure.

On the basis of the solved Ir(^{1}L)$_2$(^{2}L) single crystal structure, the diffraction peaks of 1D WAXD pattern are assigned as shown in Fig. 2. The first five diffraction peaks were assigned to

be 100, 001, 010, 011, 111 diffraction spots according to the unit cell parameter.

The comparison between the experimental and calculated results from the proposed $Ir(^1L)_2(^2L)$ single crystal structure is listed in Tab. S1. The Experimental Bragg Angles (θ_e) and Distances (d_e), and Calculated Bragg Angles (θ_c) and Distances (d_c), hkl Miller Indices of the 1D WAXD peaks assigned in Fig.2 are also listed in Tab. S1.

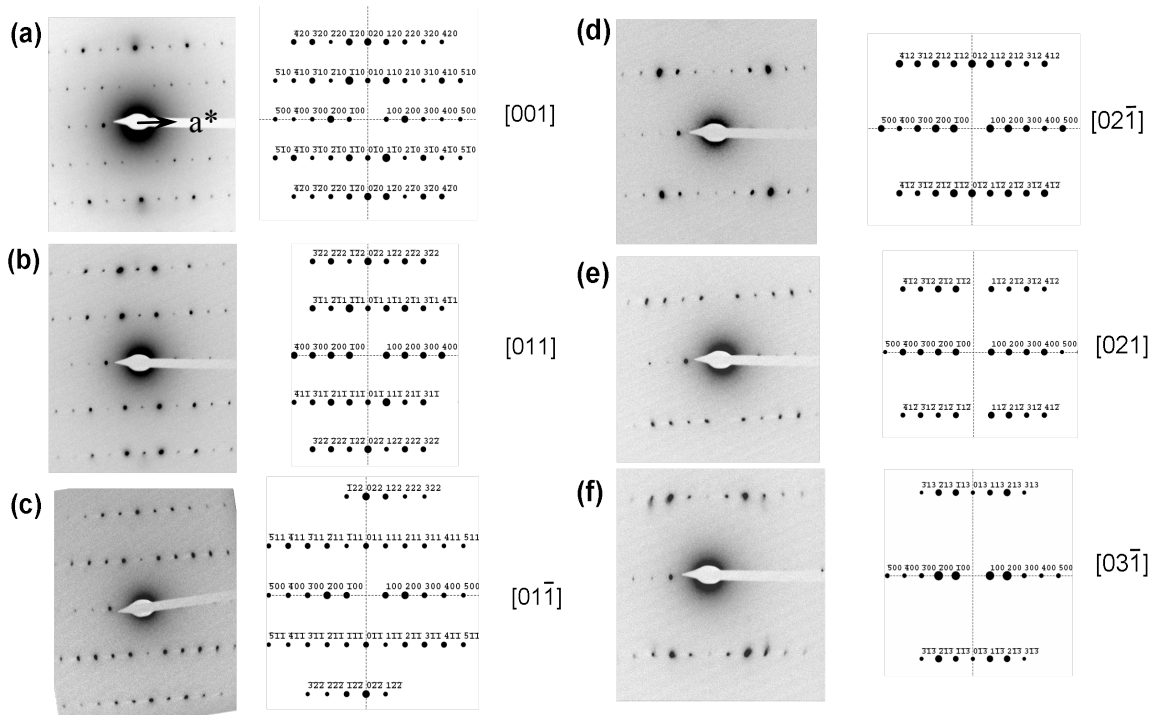

Fig. S1. Experimental and calculated ED patterns by Cerius^2 modeling package with (a) the [001] zone; (b) the [011] zone; (c) the [01$\bar{1}$] zone; (d) the [02$\bar{1}$] zone; (e) the [021] zone; (f) the [03$\bar{1}$] zone.

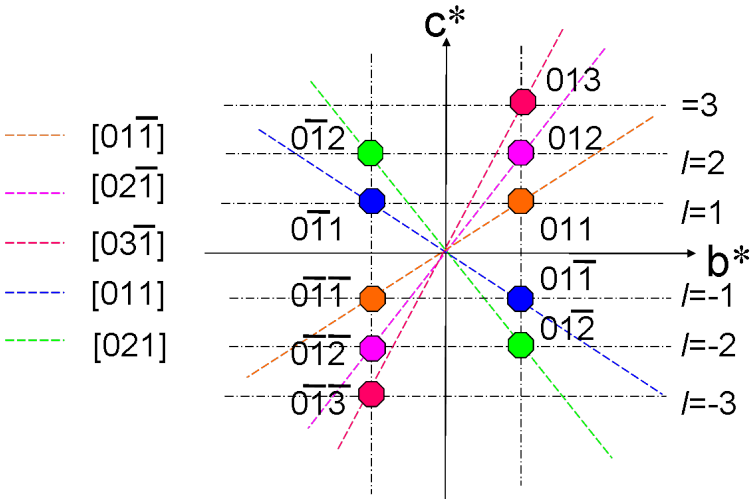

Fig. S2. 011, 012, 013, 0$\bar{1}$1, 0$\bar{1}$2 (1$\bar{1}$2) diffraction spots appeared corresponding to the [01$\bar{1}$], [02$\bar{1}$], [03$\bar{1}$], [011], [021] zone.

Table S1. Experimental bragg angles (θ_e) and distances (d_e), and calculated bragg angles (θ_c) and distances (d_c), *hkl* miller indices of the one dimensional X-ray diffraction maxima assigned in the patterns of Fig.2.

n	*hkl*	θ_e	θ_c	d_e (nm)	D_c (nm)
1	100	2.20	2.17	2.01	2.03
2	001	3.09	2.96	1.43	1.49
3	010	4.42	4.46	1.00	0.99
4	011	5.26	5.33	0.84	0.83
5	111	5.98	5.82	0.74	0.76
6	102	6.41	6.32	0.69	0.70
7	021	9.24	9.44	0.48	0.47
8	221	10.32	10.32	0.43	0.43
9	022	10.83	10.83	0.41	0.41
10	222	11.40	11.69	0.39	0.38
11	313	12.01	12.02	0.37	0.37
12	204	13.10	12.72	0.34	0.35
13	230	13.93	14.39	0.32	0.31
14	033	16.58	16.58	0.27	0.27

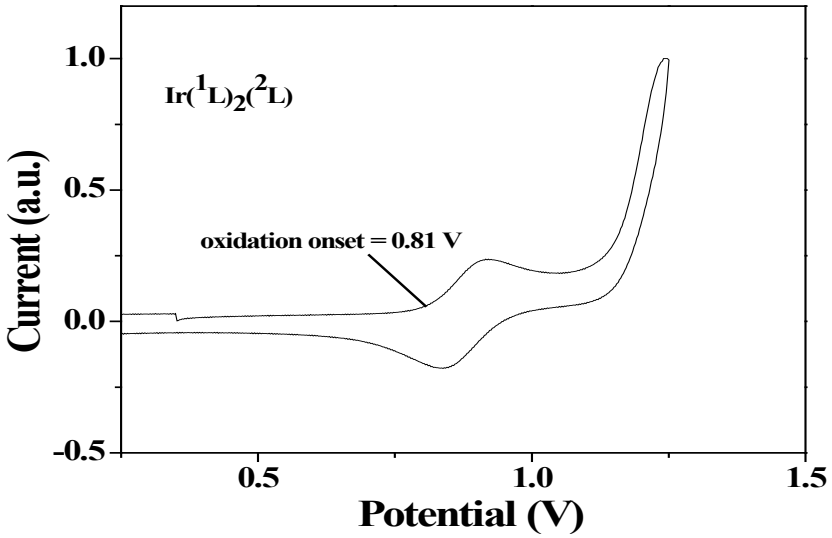

Fig. S3. Cyclic voltammogram of the complex $Ir(^1L)_2(^2L)$ in CH_2Cl_2 solution with tetra-n-butylammonium tetrafluoroborate (0.1 mol/L) as the electrolyte. (Scan rate: 10 mV/s).

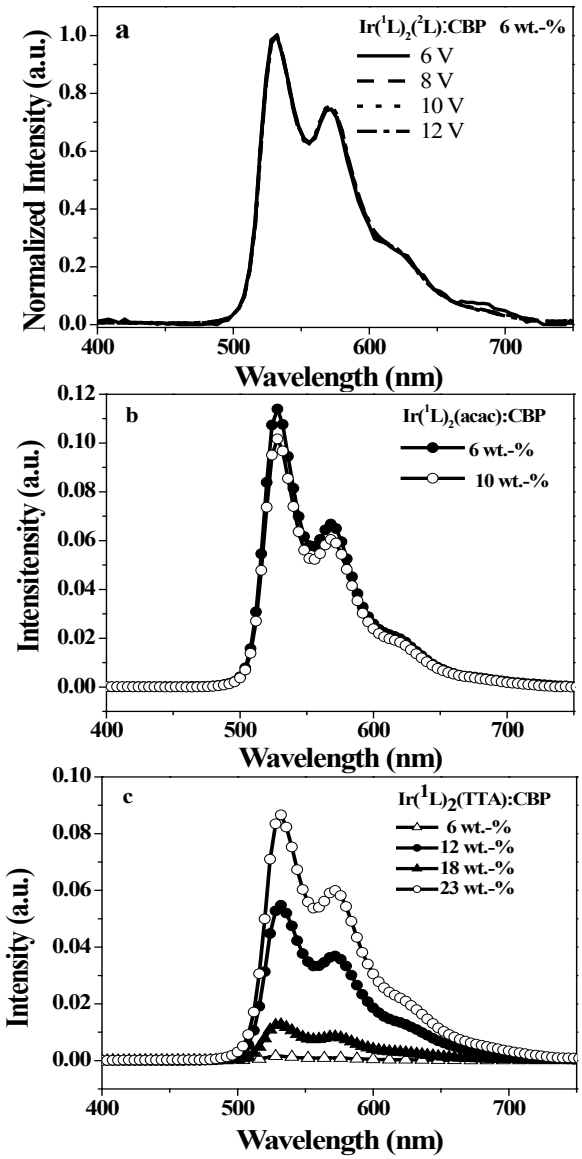

Fig. S4. EL spectra of the complexes. (a) $Ir(^1L)_2(^2L)$ at different voltages (6.0 wt.%); (b) $Ir(^1L)_2(acac)$ and (c) $Ir(^1L)_2(TTA)$ (c) with different doping concentrations. Device configuration: ITO/m-MTDATA/NPB/CBP:Complex (x wt.%)/TPBi/LiF/Al.